

Immobilization of radioactive fluoride waste in aluminophosphate glass: a molecular dynamics simulation

Ling-Wei Gao^{1,2} · Xiao-Bin Xia¹ · Xiu-Qing Xu^{1,2} · Chang-Qi Chen^{1,2}

Received: 17 January 2017/Revised: 6 November 2017/Accepted: 15 January 2018/Published online: 26 May 2018
© Shanghai Institute of Applied Physics, Chinese Academy of Sciences, Chinese Nuclear Society, Science Press China and Springer Nature Singapore Pte Ltd. 2018

Abstract Molecular dynamics (MD) simulations were conducted to investigate the structural and chemical environment of aluminum in aluminophosphate glasses. Such glasses have the potential for application in the disposal of radioactive fluoride waste from molten salt reactors (MSR). Due to the risks of studying these materials and the limitations of realistic research conditions, MD simulations were used as an alternative method to study the vitrification of radioactive fluoride waste. In the past decades, aluminophosphate glasses have been studied and they exhibit certain favorable properties for high-level radioactive waste management. This work focuses on the effects of fluorine addition on structural changes in the glass. We observed that glass with composition $P_2O_5-Al_2O_3-Na_2O-CaO$ exhibited a good performance in immobilizing fluoride at low F concentrations (approximately under 25 mol%). Significant changes were observed where PO_3F_2 units replaced PO_3F units in the glass. The four-coordinated AlO_4 units were increasingly converted into five-coordinated $[AlO_xF_y]$ with the increasing F content. The radionuclide Sr in the simulation had the tendency to form six-coordinated octahedrons in the glass. We conclude that the structural changes resulting from the fluoride

waste added to aluminophosphate glasses does not adversely affect their chemical stability at relatively low F concentrations, i.e., under 25 mol%. Hence, the use of phosphate glasses is a potential alternative method of fluoride waste disposal.

Keywords Molecular dynamics simulations · Fluoride · Aluminophosphate glasses · Immobilization

1 Introduction

The molten salt reactor (MSR) is one of the six suitable choices of reactors for Generation IV advanced nuclear energy systems [1]. These are liquid-fuel reactors using molten fluoride salts as both fuel and coolant simultaneously [1–4]. Hence, large quantities of radioactive fluoride waste are generated after the fuel cycle, which includes fluoride volatility reprocessing and vacuum distillation. This waste contains fission products (FPs) and residual fluoride salt carriers. The majority of radioactive fluoride waste types are solid-state granules or powder, which are highly corrosive and easily soluble in water [5, 6]. Therefore, it is necessary to prevent fluoride waste from being released into the environment, especially because their dissolution into water systems can cause great environmental damage. According to domestic and international research [7–12], an alternative approach to stabilize fluoride salts is glass immobilization using borosilicate or phosphate glass. This method can reduce the migration and dispersion of contaminants, radionuclides, and fluorine-inclusive waste. Although borosilicate glass has been developed for high-level waste (HLW) embedding and has been widely applied [13], it cannot embed a

This work was supported by the Strategic Pilot Science and Technology Project of Chinese Academy of Sciences (No. XDA02050).

✉ Xiao-Bin Xia
xiaxiaobin@sinap.ac.cn

¹ Shanghai Institute of Applied Physics, Chinese Academy of Sciences, Jiading Campus Shanghai 201800, China

² University of Chinese Academy of Sciences, Beijing 100049, China

large amount of fluoride owing to its low fluoride solubility.

Phosphate-based glasses [14] are generally used as biomaterials [15], substrates to immobilize waste (including radioactive and non-radioactive industrial waste) [16], and other important applications [17, 18] owing to their relatively large thermal expansion coefficient, low optical dispersion, high refractive indices, and low glass transition temperature (T_g).

Mesko et al. [10] demonstrated that iron phosphate (IP) glasses can immobilize 31 mol% SrF_2 . Sodium aluminophosphate (NaAlP) glasses have been developed at the Institute of Physical Chemistry at the Russian Academy of Sciences [12]. Yaping et al. [19, 20] showed that the NaAlP glass matrix can contain up to 20 mol% of simulated radioactive fluoride waste, and its chemical durability is better than that of borosilicate. Tiwari B et al. [21] found that Al_2O_3 , as a network intermediate added to the glass network, increases the proportion of AlPO_4 groups and, hence, improves the relatively poor chemical durability of phosphate glasses [22, 23]. In aluminophosphate glass matrices, the solubility limit of cerium oxide is 16 times higher than that of silicate glasses, while retaining the same ability for radiation damage resistance [24, 25]. Meanwhile, aluminum ingredients were found to be important in the radiation resistance properties of aluminophosphate glasses [26, 27]. Incorporation of CaO in phosphate glasses can result in reactions with fluorine. This results in the dispersion of fluorapatite in the glass, which increases its stability [28].

Diffraction studies [29–31] have demonstrated that aluminum atoms are crucially important in phosphate glasses, when four-fold coordinated Al is network former. Nevertheless, six-fold coordinated Al ions are also important and induce significant changes in properties. Two different types, tetrahedrally- and octahedrally coordinated aluminum, have been observed in the local structures of aluminophosphate glasses by nuclear magnetic resonance (NMR) or Raman spectroscopy [26, 32]. Certain ^{19}F magic-angle spinning (MAS) NMR studies of aluminosilicate glasses [33] have shown that Al–F bonds exist in F-containing glasses, while Si–F bonds exist in very high F-content glasses. This indicates that Al–F bonds are preferred to Si–F bonds when both Al and Si are present in high F-content glasses. Similarly, fluorinated silicate glasses show a very small amount of F–Si bonds in molecular dynamics (MD) simulations [34, 35]; therefore, they are separated into phosphosilicate-rich and Na/Ca/F-rich regions at medium-length scales [36].

The waste from MSRs has very complex compositions and the glass solidification of MSR waste is still in preliminary stages of research. This study begins with simple waste components in waste vitrification and uses an MD

simulation method to understand the immobilization of fluoride waste. As part of the fission fragment elements, Sr is usually chosen to act as a simulated radioactive fission product. Variable amounts of SrF_2 are added to the glass to investigate its structural changes. This also enables useful information to be gained from a certain relatively simple experiment.

In this work, we concentrate on the effects of amalgamative fluorine on the structure of phosphate-based glasses. The MD simulation approach is ideal and has been widely used to investigate the structural and dynamical properties of several different types of glasses [37–40]. It provides an alternative method for investigating the properties of molten glass [41], thus, enabling the comprehension of the specific contributions of selected structural units on material properties at the atomistic level. We use two phosphate glass compositions with different fluorine contents. The interatomic forces are calculated by a classical MD simulation, providing vital information on atomic structure and properties.

2 Simulation Method

Three independent initial quasi-random configurations were generated. All of these were chosen to have the same ratio of numbers of P atoms to Al atoms ($n(\text{Al}_2\text{O}_3)/n(\text{P}_2\text{O}_5) = 0.5$). One configuration, with 15 mol% SrF_2 (hereafter called F15), was obtained by placing 459 atoms (comprising $34\text{P}_2\text{O}_5$ - $23\text{Na}_2\text{O}$ - 11CaO - $17\text{Al}_2\text{O}_3$ - 15SrF_2 formula units) randomly into a cubic box of side length of 18.3894 Å, corresponding to the experimental density of 2.80 g cm^{-3} . The second configuration had 25 mol% SrF_2 (hereafter called F25) in a cubic cell with 18.1088-Å sides, containing 440 atoms (with the composition $30\text{P}_2\text{O}_5$ - $20\text{Na}_2\text{O}$ - 10CaO - $15\text{Al}_2\text{O}_3$ - 25SrF_2) at a density of 3.00 g cm^{-3} . The third model had no SrF_2 (hereafter called F0) in a cubic cell with 18.748-Å sides containing 487 atoms (with a composition of $40 \text{ P}_2\text{O}_5$, $27 \text{ Na}_2\text{O}$, 13 CaO , $20 \text{ Al}_2\text{O}_3$) at a density of 2.55 g cm^{-3} .

The exact compositions are given in Table 1. The size of the box was chosen to give the appropriate density and was kept constant throughout the simulation.

The force field used in this work is based on the Buckingham potential, given by

$$E_{ij}(r_{ij}) = A_{ij} \exp(-r_{ij}/\rho_{ij}) - C_{ij}/r_{ij}^6 + q_i q_j / r_{ij}, \quad (1)$$

where E_{ij} is the potential between atoms i and j , A_{ij} , ρ_{ij} , and C_{ij} are the parameters of the i - j interaction, while r_{ij} is the distance between atoms i and j . Cubic periodic boundary conditions are used with a cutoff of 6 Å, with the Buckingham terms evaluated in real space.

Table 1 Simulated compositions (in SrF₂ mol%) and their densities and sizes

Composition	P ₂ O ₅	Na ₂ O	CaO	Al ₂ O ₃	SrF ₂	Density (g cm ⁻³)	Number of atoms	Cell size (Å)
F0	40	27	13	20	0	2.55	487	18.7480
F15	34	23	11	17	15	2.80	459	18.3894
F25	30	20	10	15	25	3.00	440	18.1088

In addition, three-body forces, including a harmonic potential, are applied to the potential parameters for O–P–O and P–O–P bond bending interactions [37] in the form of

$$E_{iji}(\theta) = 1/2k_{iji}(\theta - \theta_{iji}), \tag{2}$$

where *j* is the type of element of the central atom, *k_{iji}* is the three-body force constant and *θ_{iji}* is the reference bond angle. Potential parameters of the aluminophosphate glasses are listed in Table 2.

Each random model was started as an MD run in an NVT (constant number of particles, volume, and temperature) ensemble at 3000 K for a certain time (typically ~ 100 ps), beyond which the glass were melt, until the model was well equilibrated. The simulations were performed with a 1 fs time step. Then, each model was run at temperatures 2000, 1000, 500, and 300 K for 50 ps, which corresponds to a cooling rate of 50 K/ps. Although this simulated cooling rate is significantly faster than that used to prepare the experimental glasses, this order of magnitude of cooling rate is in agreement with first

principles [35, 36, 42–44] and classical [38, 41] MD simulations.

3 Results and discussion

3.1 Partial radial distribution function and coordination numbers

The partial radial distribution function (RDF) is commonly used to investigate the characteristics of the short-range order. The RDF describes the variation of the probability density as a function of distance from a specified particle. The formula for the RDF is as follows:

$$g_{ij}(r) = \frac{V}{N_i N_j} \sum_j \frac{n_{ij}(r - \Delta r/2, r + \Delta r/2)}{4\pi r^2 \Delta r}, \tag{3}$$

where *V* is the volume of the simulation cell, while *N_i* and *N_j* are the total numbers of ions *i* and *j*, respectively. The term *n_{ij}(r - Δr/2, r + Δr/2)* is the average number of ion *j* surrounding ion *i* within the distance of *r ± r/2*. The RDF

Table 2 Potential parameters of flourophosphate glasses [45–53]

Pair	<i>A_{ij}</i> (ev)	<i>ρ_{ij}</i> (Å)	<i>C_{ij}</i> (evÅ ⁶)	References	Pair	<i>A_{ij}</i> (ev)	<i>ρ_{ij}</i> (Å)	<i>C_{ij}</i> (evÅ ⁶)	References
Buckingham potential									
Na–O	1226.800	0.3065	0	[46]	Ca–F	1272.800	0.3000	0	[45]
Ca–O	8668.750	0.2500	0	[45]	Ca–P	1462.500	0.3000	0	[45]
P–O	887.340	0.3700	0	[53]	Ca–Al	1406.250	0.3000	0	[45]
Al–O	3293.750	0.2500	0	[45]	Al–F	43851.020	0.1610	0	[51]
Sr–O	2026.613	0.3100	0	[52]	Al–Al	10689.029	0.1420	0	[51]
O–O	454.343	0.3600	0	[45]	Al–P	1018.750	0.3000	0	[45]
F–O	662.500	0.3200	0	[45]	Sr–Sr	16574.664	0.2600	0	[49]
Na–Na	5000.000	0.2900	0	[47]	Sr–F	715.410	0.3400	0	[50]
Na–F	706.250	0.2900	0	[47]	F–F	135253.000	0.1800	0	[51]
Na–P	649.246	0.2900	0	[48]	F–P	452.500	0.3640	0	[45]
Ca–Ca	2412.500	0.3000	0	[45]	P–P	831.250	0.3000	0	[45]
Three-body potential									
		<i>k_{iji}</i> (eV rad ⁻²)				<i>θ_{iji}</i>			
O–P–O		3.3588				109.470000			
P–O–P		7.6346				141.179333			

describes the structural ordering of the slag in different ranges and also provides fundamental structural information including average bond lengths. The RDFs are shown in Fig. 1, while Table 3 shows the average interatomic distances of atoms (which is our main focus and discussed later). In these glasses, the bond lengths for P–O and Al–O were centered at 1.55 and 1.75 Å, respectively, and were similar to those of the other aluminophosphate glasses measured experimentally [31, 54]. The average Al–F and P–F bond distances were 1.55 and 1.81 Å, respectively,

which is close to that of the other MD simulations [35, 36, 47], where the Al–F and P–F bond lengths were found to be approximately 1.59 and 1.83 Å.

The coordination number can be defined using the $g(r)$ of the RDF and it can be calculated by integrating the corresponding $g(r)$ curve to the first valley, using the following formula:

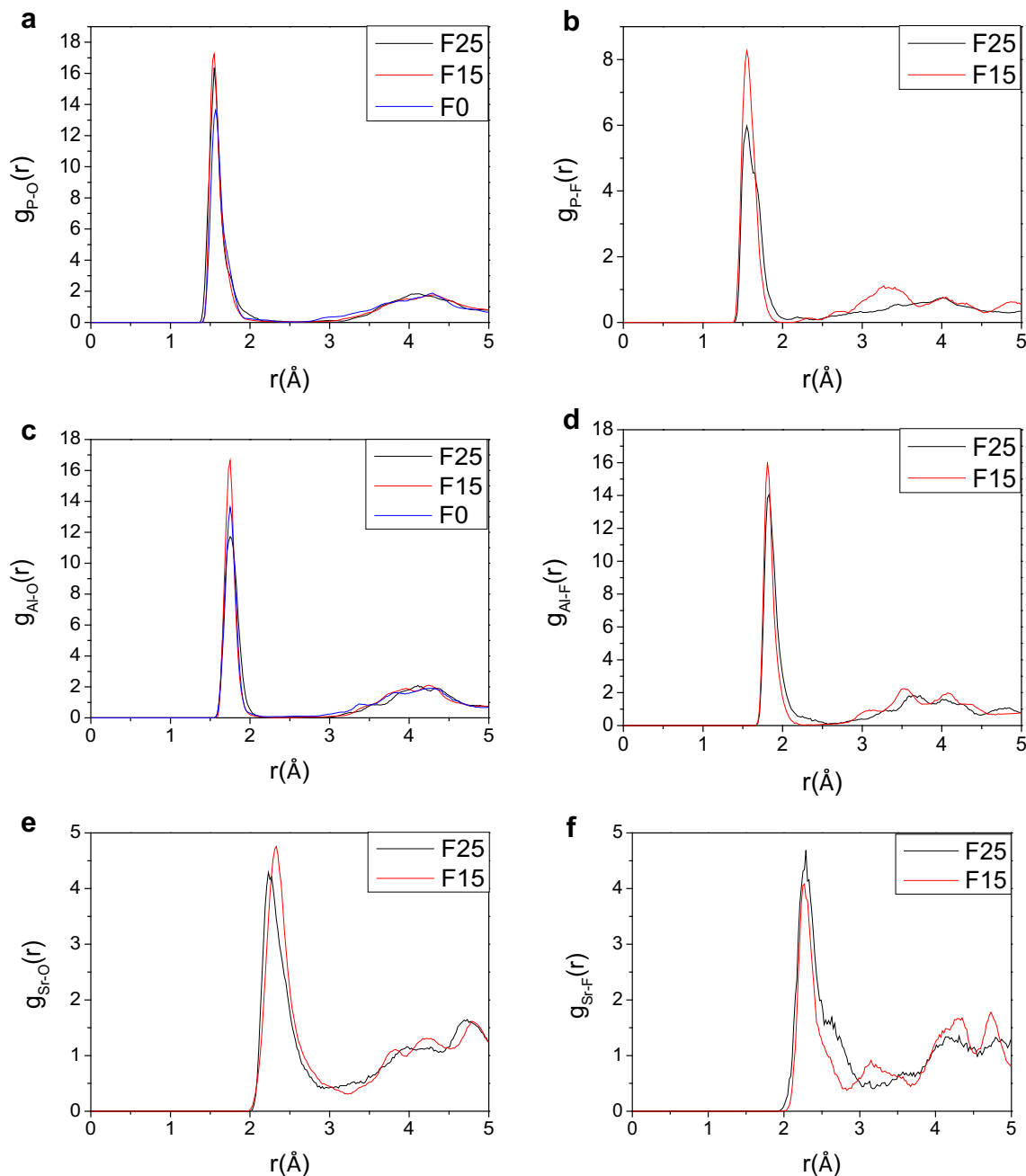


Fig. 1 (Color figure online) RDFs of cation–anion: P–O (a), P–F (b), Al–O (c), Al–F (d), Sr–O (e), and Sr–F (f) pairs. In the figures, configurations F0, F15, and F25 correspond to the blue, red, and black lines, respectively

Table 3 Average interatomic distances of the studied aluminophosphate glasses

Sample no.	Pair							
	P–O	Al–O	Sr–O	P–F	Al–F	Sr–F	Sr–P	Sr–Al
F15	1.55	1.75	2.33	1.55	1.81	2.27	3.59	3.43
F25	1.55	1.75	2.27	1.55	1.83	2.29	3.57	3.29

$$N_{ij}(r) = \frac{4\pi N_j}{V} \int_0^r g_{ij}(r)r^2 dr. \tag{4}$$

The studied average coordination numbers are listed in Table 4 and others are analyzed in detail in the following sections. Considering both the oxygen and fluorine coordination, the coordination number of phosphorus was close to 4 and the coordination number of aluminum was more than 4, due to penta-coordinate and hexa-coordinate Al. The coordination numbers of calcium and sodium (calculated as the sum of the F and O contributions) were close to 6 and 7, respectively. The focused average coordination numbers of strontium were in the range of 5.43–6.10. Obviously, the mean oxygen coordination numbers of metal cations decrease with the addition of fluoride anions, where F competes with O, resulting in an increase in the coordination number of F.

3.2 Local environments of phosphorus

For both compositions containing F, the first peak in the phosphorus–oxygen partial radial distribution function ($g(r)$; Fig. 1a) shows that the P–O distance is 1.55 Å. In an F-free glass (F0), the distance is 1.57 Å, which is in agreement with the observed nearest-neighbor distances reported in other papers [41, 55]. Usually, in an F-free glass the P–O coordination number is exactly four, reflecting the tetrahedral structures around the P atoms. In this study, the P–O coordination number was slightly over four, at 4.004. We found lower oxygen coordination numbers: 3.83 for

F15 and 3.76 for F25. By examining $g_{P-F}(r)$ (Fig. 1b) and the P–F coordination numbers, 0.17 for F15 and 0.28 for F25, we know that there is an amount of P–F bonding, and that fluorine atoms replace one of the oxygen atoms in the PO₄ units, retaining the tetrahedral structure around the phosphorus atoms at low F concentrations. In general, the phosphorus atoms are essentially four-coordinated, which both oxygen and fluorine are considered at the same time [35]. When P–F bonding occurs, one of the fluorine atoms takes the place of one of the oxygen atoms in the PO₄ unit, generating a PO₃F tetrahedron. However, at high F concentration (F25), the P–X (O, F) coordination number exceeds four (4.04), indicating that five-coordinate PO₃F₂ indeed exists in the structural units breaking the structure of PO₄ units. Generally, the aluminophosphate network combines with the corner sharing of the PO₄ and AlO₄ tetrahedral units. The network connectivity (NC) can be used to show the mean number of bridging oxygen atoms in PO₄ tetrahedral units. The presence of PO₃F₂ breaks the glass structure by reducing the NC such that the glass system becomes unstable. Segmental examples of these structural units are illustrated in Fig. 3.

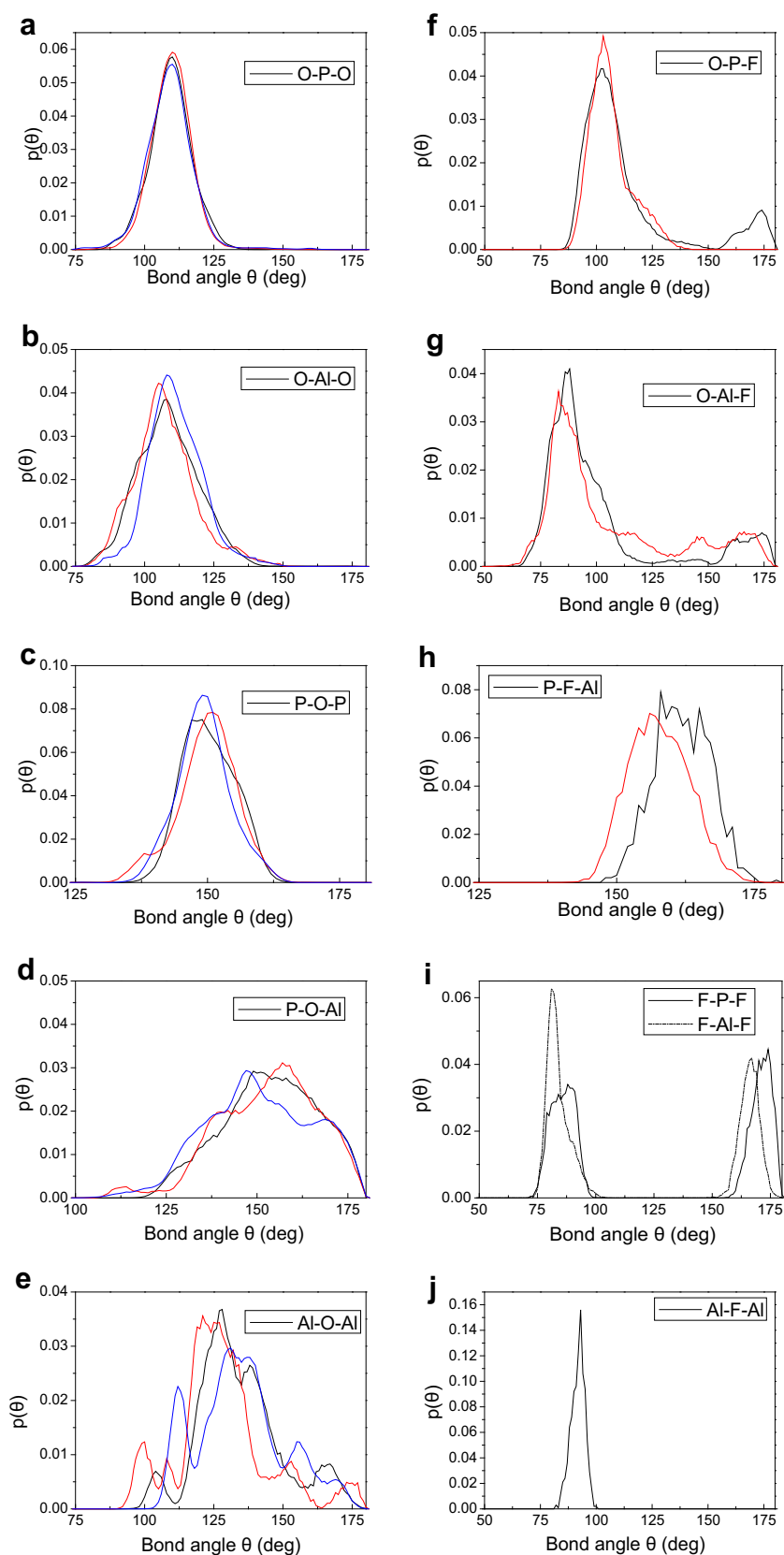
At both F-concentrations, no bridging F atoms (atoms in a P–F–P bridge) were observed, due to the single negative charge of F ions. It is difficult to charge-balance two phosphorus atoms, due to the double negative charge of the oxygen atom [36]. Meanwhile, rare-bridging F atoms appear as P–F–Al in F15 and F25 (Fig. 2h). To investigate the tetrahedral nature of the phosphate units, the O–P–O and P–O–P bond-angle distributions were calculated

Table 4 Average coordination numbers of the studied aluminophosphate glasses

Sample no.	Pair								
	P–O	Al–O	Ca–O	Na–O	Sr–O	P–F	Al–F	Sr–F	Na–F
F0	4.00	4.01	5.70	6.40	0	0	0	0	0
F15	3.83	3.91	5.20	6.00	5.10	0.17	0.50	0.33	0.68
F25	3.76	3.69	4.90	5.50	4.90	0.28	0.99	1.20	1.47

Sample no.	Pair							
	Ca–F	P–Na	P–Ca	P–Sr	Al–Na	Al–Ca	Al–Sr	F–F
F0	0	3.96	0.85	0	3.26	0.61	0	0
F15	0.56	3.29	0.75	0.98	3.01	0.50	0.70	0.44
F25	1.04	2.97	0.75	1.86	2.72	0.43	1.04	1.12

Fig. 2 (Color figure online) Bond-angle distributions for F0 (blue), F15 (red), and F25 (black) for O–P–O (a), O–Al–O (b), P–O–P (c), P–O–Al (d), Al–O–Al (e), O–P–F (f), O–Al–F (g), P–F–Al (h), F–P–F (i) and Al–F–Al (j)



(Fig. 2a and c), showing an O–P–O distribution peak (110°) close to the ideal PO_4 tetrahedral angle (109.5°) and a P–O–P distribution peak (near 149°) exceeding the ideal tetrahedral angle (141.2°) for both compositions. The O–P–F bond-angle distributions (Fig. 2f) peaked at slightly lower angles (105°), as the substitution of F atoms by O atoms alters PO_3F to be slightly different from PO_4 in the glass structure. However, in F25, there was another distribution peak (174°), showing that an F atom was almost in line with an O atom.

This case is also shown in Fig. 2i, where F–P–F bond-angle appears, indicating that there was a PO_3F_2 unit in the simulated glass. As the presence of PO_3F_2 is not supported by empirical evidence, further studies need to be carried out to examine this result.

3.3 Local environments of aluminum

In F0, the Al–O coordination number was 4.008, implying that the majority of the aluminum atoms were in a tetrahedral coordination. In the other compositions, the coordination numbers were 3.91 (for F15) and 3.69 (for F25). Nevertheless, the Al–F coordination numbers were 0.50 for F15 and 0.99 for F25. The Al–X (O, F) coordination number exceeded four in both compositions: 4.41 for F15 and 4.68 for F25.

Similarly to silicon in glass, phosphorus and aluminum are both network formers and have tetrahedral coordination with oxygen [55] in F-free glass. In other studies, aluminum atoms were found to be primarily in tetrahedral coordination state in aluminophosphate glasses with increasing alumina contents, whereas octahedrally coordinated aluminum atoms play a major role with a small quantity of Al_2O_3 contents [56–59]. However, Al–F bonding is slightly different from the P–F bonding, because F atoms not only replace one oxygen atom in an AlO_4 unit, but replace other oxygen atoms as well to create five-coordinate $[\text{AlO}_x\text{F}_y]^{n-}$, leading to more F atoms being included in AlO_4 . Similarly, Stamboulis et al. [33] studied the ^{19}F MAS NMR of calcium fluoro-alumino-silicate glasses and found that as glass it forms $[\text{AlO}_x\text{F}_y]^{n-}$, where $x = 3-6$, $y = 6 - x$, and n is the charge of the total complex in Al(IV), Al(V), and Al(VI) coordinate states. We believe that some of the F atoms replace oxygen atoms to form AlO_3F , while others intrude AlO_4 units and transform them to AlO_4F in low F concentrations. For the F25 composition, increasing numbers of F atoms bonded to aluminum atoms, creating more non-tetrahedrons such as AlO_3F_2 , AlO_3F_3 , and others. These need to be examined in further F-NMR experiments. Segmental examples of these structural units are illustrated in Fig. 3. A large number of P–O–P bonds are replaced by P–O–Al bonds [60] which play a significant role in increasing the network connectivity and

nuclide containment for phosphate-based glasses, enabling their modification for specific applications.

To investigate the tetrahedral nature of the phosphate units, the O–Al–O bond-angle distributions were calculated (Fig. 2b). These showed distribution peaks of 108° for F25 and 105° for F15, which are close to the ideal tetrahedral angle (109.5°). As can be seen in Fig. 2d and e, the P–O–Al and Al–O–Al bond-angle distributions were scattered. The O–Al–F bond-angle distributions are shown in Fig. 4b, with a first peak (approximately 85°) that is slightly low. We believe that it is possible that the replacement of F atoms and the simulation process do not use three-body potential for O–Al–O. Considering the Al(V) and Al(VI) coordinate states, the angle distribution curve continues up to 180° . Figure 2i and j provides consequential information about the Al–F interaction. At low F concentration (F15), there were no bridging F atoms observed (atoms in an Al–F–Al bridge), and it was the same for the F–Al–F bond-angle distributions. This is different from the F25 composition, where bridging F atoms (atoms in an Al–F–Al bridge) were observed, albeit in small numbers, while the F–Al–F bond-angle distributions showed that at least two F atoms bonded to an Al atom.

3.4 Fluorine bonding and coordination numbers

In the F15 composition, the F–P coordination number was 0.39, i.e., 2 out of 5 fluorine atoms bonded to a phosphorus atom. In the F25 composition, 17 of the 50 fluorine atoms were bonded, with an F–P coordination number of 0.34. This is in contrast with Christie et al. [35], who calculated much lower F-concentrations. In their study, three of the four fluorine atoms were bonded to a phosphorus atom for F2, and three of the six fluorine atoms were bonded for F6, indicating that the major F atoms impose a constraint in PO_3F .

As with F–P, the F–Al coordination number was 0.57 in the F15 composition, where 17 of the 30 fluorine atoms were bonded to aluminum. In the F25 composition, 30 of the 50 fluorine atoms were bonded, with an F–P coordination number of 0.59. The fluorine-modifier bonding in both compositions indeed has different characteristics. For the F15 composition, the F–Na bond length is about 2.15 \AA , which is slightly shorter than the 2.19 \AA of the F25 composition. The F–Na coordination number is 1.04 for F15 and 1.18 for F25. The peaks in the corresponding partial pair distribution functions, $g_{\text{Sr-F}}(r)$ (Fig. 1f) are broader than the typical F–P/Al peak, indicating substantial disorder in the local environments [35]. Similarly, the F–Ca bond length was about 2.21 \AA in the F15 composition, which is longer than the 2.15 \AA of the F25 composition. The F–Ca coordination numbers were 0.21 for F15 and 0.34 for F25.

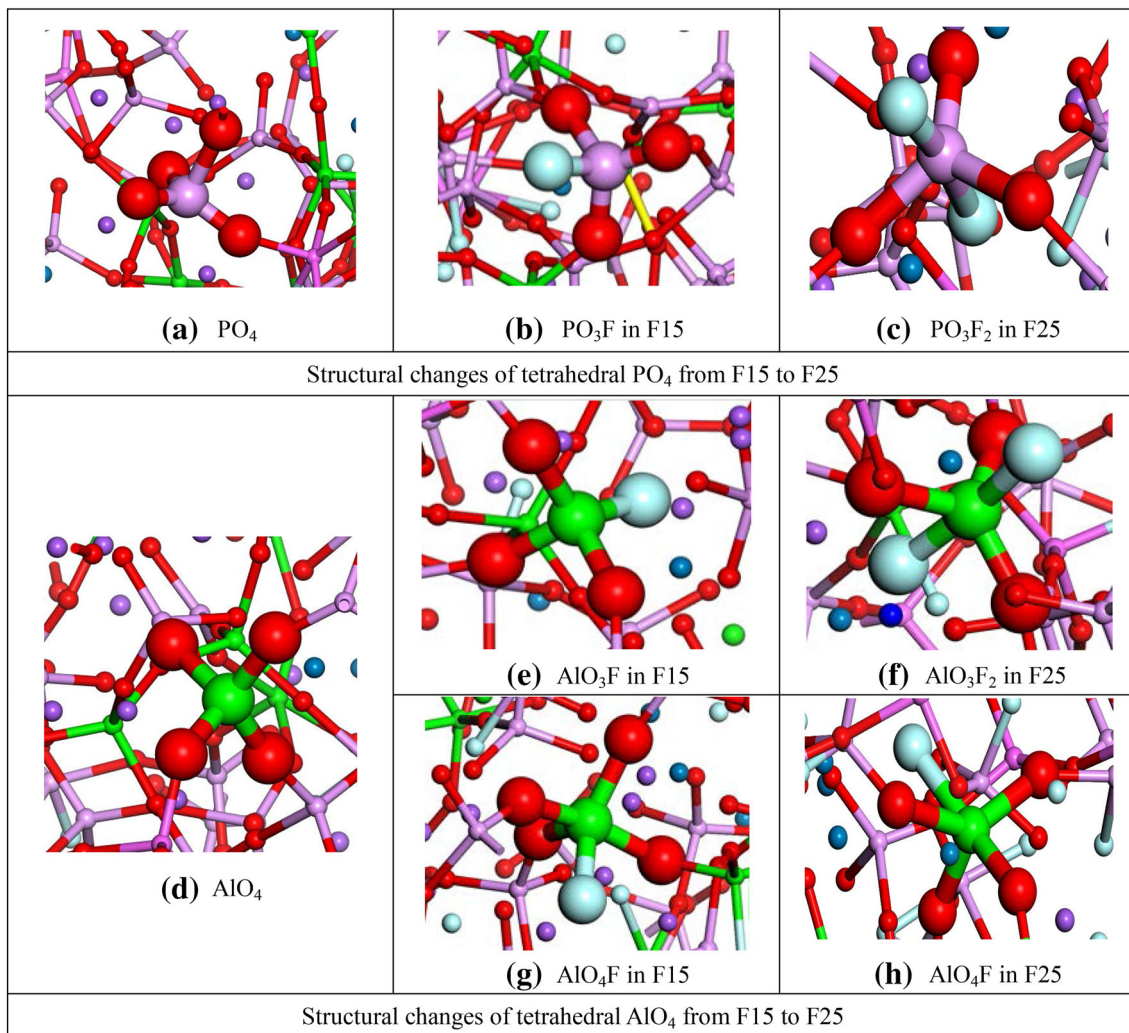


Fig. 3 (Color figure online) Examples of structural changes, from tetrahedral to hexahedral. The surrounding atoms have been shrunk for clarity (P = magenta, O = red, F = silver, Al = green). Structural changes of tetrahedral PO_4 from F15 to F25, **a** PO_4 , **b** PO_3F in F15,

c PO_3F_2 in F25. Structural changes of tetrahedral AlO_4 from F15 to F25, **d** AlO_4 , **e** AlO_3F in F15, **f** AlO_3F_2 in F25, **g** AlO_4F in F15, **h** AlO_4F in F25

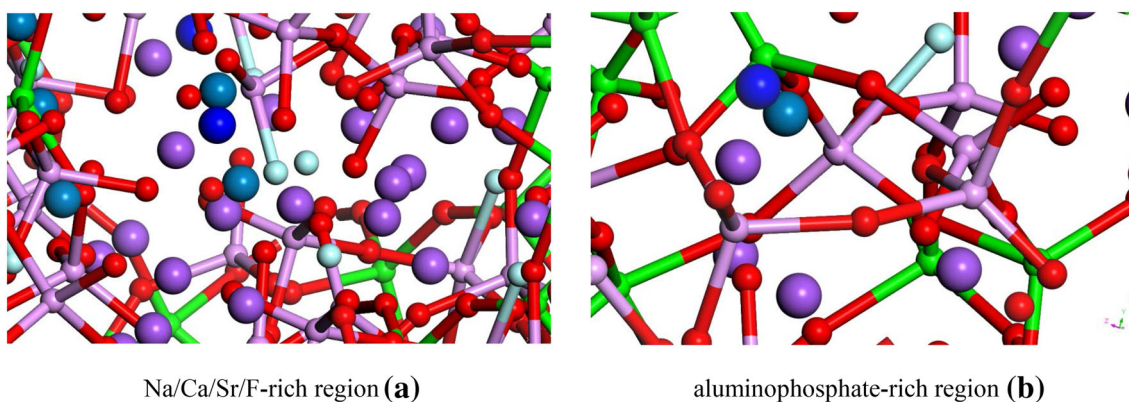
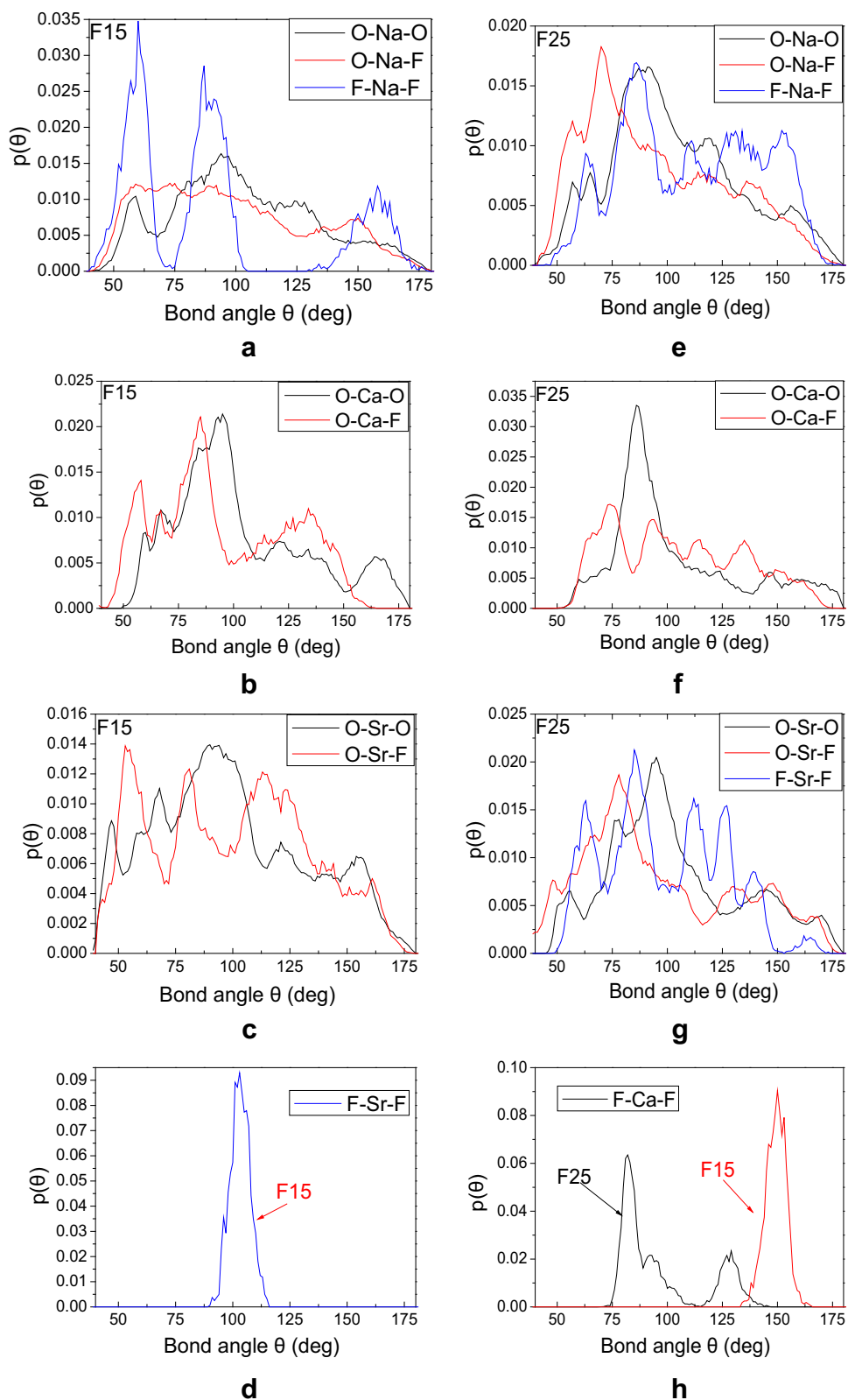


Fig. 4 (Color figure online) Aluminophosphate-rich and Na/Ca/Sr/F-rich regions in aluminophosphate glass (P = magenta, O = red, F = silver, Al = green, Na = purple, Ca = dark blue, Sr = mid blue). Na/Ca/Sr/F-rich region (**a**). Aluminophosphate-rich region (**b**)

Fig. 5 (Color figure online) Bond angle distributions of O–M–O, O–M–F and F–M–F for F15 and F25. M = Na, Ca, and Sr



As radionuclides in the simulation, Sr atoms are immobilized in the glass, and their release into the environment needs to be avoided. For the F15 composition, the

F–Sr bond length was about 2.27 Å, slightly shorter than the 2.29 Å of the F25 composition. The F–Sr coordination number was 0.17 for F15 and 0.60 for F25. The number of

F atoms surrounding Sr atoms increases with the increase of the F-concentration.

The F–F coordination numbers (Table 4) were observed to increase with the addition of SrF₂, indicating that the amount of fluorine atoms is increasing around fluorine atoms. The results suggest a tendency of fluorine atoms to concentrate with each other. The coordination numbers of P–Na/Ca and Al–Na/Ca decrease with the addition of SrF₂, which shows that the modified ions tend to deviate from the network former atoms. Doping with fluorine results in the separation of the glass into aluminophosphate-rich and Na/Ca/Sr/F-rich regions, as shown by Fig. 4.

3.5 Simulated atoms and modifier atom bonding

Table 4 shows the Na and Ca coordination numbers, considering both oxygen and fluorine in the first coordination shell. The coordination numbers for Na are in the range of 6.4–6.97, and in the range of 5.7–5.94 for Ca, taking the coordination to both oxygen and fluorine into account. This implies that six and seven are the most common coordination numbers for sodium, and six is the most common coordination number for calcium. The state of strontium is similar to that of calcium, with coordination numbers of 5.43 for F15 and 6.1 for F25. Strontium atoms were observed to be concentrated on aluminophosphate-rich regions by forming 0.06SrF₂·0.98Sr₃(PO₄)₂·AlPO₄ at low F concentrations.

However, strontium atoms tend to enter into aluminophosphate-rich regions coordinating with more aluminate in the form of 0.8SrF₂·1.06Sr₃(PO₄)₂·1.9AlPO₄ at high F concentration. This is because strontium competing favorably with calcium/sodium to bond the AlO₄ with the enhancement of strontium atoms. Further studies need to consider the real radionuclide, instead of the non-radionuclide, to achieve a more realistic simulation.

Figure 5 shows the O–M–O, O–M–F, and F–M–F bond angle distributions, where M represents the modifiers of sodium, calcium, and the simulated radionuclide strontium. The O–M–O, O–M–F, and F–M–F distributions follow a similar shape with a very broad distribution of angles (~ 60–100°). Nevertheless, as the F–M–F distributions correspond to a very small single digit number of bond angles, the F–Ca–F and F–Sr–F distributions merge into a single peak. These distributions indicate a wide range of bonding environments [35], and that the structure of the first coordination shell around the positive valence atoms is octahedral. An anticipated six-coordinated octahedron is expected to show bond angles at 90° and 180°, as the coordination number of Ca is slightly less than six and the coordination number of Na is close to seven, resulting in the slight shrinking of these bond angles.

4 Conclusion

We used MD simulation to determine the structural changes in aluminophosphate-based glasses with different fluorine concentrations. We conclude that this study likely provides useful information on the effect of fluorine doping on glass stability. First, in low F concentrations, an oxygen atom in a PO₄ tetrahedron is replaced by a non-bridging fluorine atom, transforming PO₄ to PO₃F, resulting in a reduction in glass network connectivity. The tetrahedral environment of phosphorus atoms is maintained at low F concentrations, and its structure does not remain solid at high F concentrations (more than 25 mol%), because fluorine breaking the network connections. In contrast, AlO₄ performs differently from PO₄ due to the presence of [AlO_xF_y] with Al(IV), Al(V), and Al(VI) coordinate states, which enables more fluorine to increase the occlusion capacity of solidified fluoride waste. Furthermore, Al₂O₃ can be added to improve the chemical resistance of phosphate glasses (by replacing the P–O–P bonds with more chemically durable P–O–Al bonds) for the specific application of radioactive fluoride waste treatment. Hence, we expect that phosphate-based glasses will take precedence over silicate-based glasses in radioactive fluoride waste disposal. Moreover, the MD simulation applied in this work was efficient and provided a theoretical basis for the study of the solidification of radioactive waste, especially in complicated environments, which most laboratories could not afford to perform. However, we recommend that simulations should be combined with experiments, which can accelerate the development of radioactive waste disposal.

References

1. S.Q. Qiu, D.L. Zhang, G.H. Su et al., Research on inherent safety and relative key issues of a molten salt reactor. *Atomic Energy Sci. Technol.* **43**, 64–75 (2009)
2. B. Cai, K. Wang, L. Sun et al., Experimental study and numerical optimization on a vane-type separator for bubble separation in TMSR. *Prog. Nucl. Energy* **74**, 1–13 (2014). <https://doi.org/10.1016/j.pnucene.2014.02.007>
3. J. Tian, X.B. Xia, C. Peng et al., Impact analysis of criticality safety for 10-MWt solid thorium-based molten salt reactor spent nuclear fuel storage system. *Nucl. Sci. Tech.* **38**(5), 50602 (2015). <https://doi.org/10.11889/j.0253-3219.2015.hjs.38.050602>
4. Z.H. Zhang, X.B. Xia, J. Cai et al., Simulation of radiation dose distribution and thermal analysis for the bulk shielding of an optimized molten salt reactor. *Nucl. Sci. Tech.* (2015). <https://doi.org/10.13538/j.1001-8042/nst.26.040603>
5. D.D. Siemer, Molten salt breeder reactor waste management. *Nucl. Technol.* **185**, 100–108 (2014). <https://doi.org/10.13182/NT12-164>
6. O.R.N. Lab, *Identification and Evaluation of Alternatives for the Disposition of Fluoride Fuel and Flush Salts from the Molten Salt*

- Reactor Experiment at Oak Ridge National Laboratory* (Tennessee. Office of Scientific & Technical Information Technical Reports, Oak Ridge, 1996)
7. D.E. Day, Z. Wu, C.S. Ray et al., Chemically durable iron phosphate glass wasteforms. *J. Non-Cryst. Solids* **241**, 1–12 (1998). [https://doi.org/10.1016/S0022-3093\(98\)00759-5](https://doi.org/10.1016/S0022-3093(98)00759-5)
 8. I.W. Donald, B.L. Metcalfe, S.K. Fong et al., A glass-encapsulated calcium phosphate wasteform for the immobilization of actinide-, fluoride-, and chloride-containing radioactive wastes from the pyrochemical reprocessing of plutonium metal. *J. Nucl. Mater.* **361**, 78–93 (2007). <https://doi.org/10.1016/j.jnucmat.2006.11.011>
 9. M.I. Ojovan, W.E. Lee, Naturally occurring radionuclides—an introduction to nuclear waste immobilisation—Chapter 5. *Introd. Nucl. Waste Immobil.* **3**, 43–52 (2005)
 10. M.G. Mesko, D.E. Day, B.C. Bunker, Immobilization of CsCl and SrF₂ in iron phosphate glass. *Waste Manag.* **20**, 271–278 (2000). [https://doi.org/10.1016/S0956-053X\(99\)00331-1](https://doi.org/10.1016/S0956-053X(99)00331-1)
 11. X. Feng, M.J. Schweiger, H. Li et al., Retention of sulfur, phosphorus, chlorine, and fluorine in Hanford Phase II vendor LLW glasses. Conference of SPECTRUM '96, Seattle, USA, 18–23 Aug 1996 (1996)
 12. Y.G. Lavrinovich, M.V. Kormilitsyn, V.I. Kononov et al., Vitrification of chloride wastes in the pyroelectrochemical method of reprocessing irradiated nuclear fuel. *At. Energy* **95**, 781–785 (2003). <https://doi.org/10.1023/B:ATEN.0000016764.68862.5f>
 13. I.W. Donald, B.L. Metcalfe, R.N.J. Taylor, The immobilization of high level radioactive wastes using ceramics and glasses. *J. Mater. Sci.* **32**, 5851–5887 (1997). <https://doi.org/10.1023/A:1018646507438>
 14. R.J. Kirkpatrick, R.K. Brow, Nuclear magnetic resonance investigation of the structures of phosphate and phosphate-containing glasses: a review. *Solid State Nucl. Magn. Reson.* **5**, 9–21 (1995). [https://doi.org/10.1016/0926-2040\(95\)00042-0](https://doi.org/10.1016/0926-2040(95)00042-0)
 15. J.C. Knowles, Phosphate based glasses for biomedical applications. *J. Mater. Chem.* **13**, 2395–2401 (2003). <https://doi.org/10.1039/B307119G>
 16. J.R. Van Wazer, Phosphorus and its compounds, INTERSCIENCE. (1958)
 17. T. Nomura, K. Masui, G. Nakagawa, Anion-selective properties of alkali metal-free lead phosphate glasses containing silver chloride and their application in an ion-selective electrode. *Anal. Chim. Acta* **237**, 135–140 (1990). [https://doi.org/10.1016/S0003-2670\(00\)83910-0](https://doi.org/10.1016/S0003-2670(00)83910-0)
 18. R.K. Brow, Review: the structure of simple phosphate glasses. *Journal of Non-Crystalline Solids* **s 263–264**, 1–28 (2000). [https://doi.org/10.1016/S0022-3093\(99\)00620-1](https://doi.org/10.1016/S0022-3093(99)00620-1)
 19. Y.P. Sun, X.B. Xia, Y.B. Qiao et al., Properties of phosphate glass waste forms containing fluorides from a molten salt reactor. *Nucl. Sci. Tech.* **27**, 96–102 (2016). <https://doi.org/10.1007/s41365-016-0059-9>
 20. Y.P. Sun, X.B. Xia, Y.B. Qiao et al., Immobilization of simulated radioactive fluoride waste in phosphate glass. *Sci. China Mater.* **59**, 279–286 (2016). <https://doi.org/10.1007/s40843-016-5010-x>
 21. B. Tiwari, M. Pandey, V. Sudarsan et al., Study of structural modification of sodium aluminophosphate glasses with TiO₂ addition through Raman and NMR spectroscopy. *Phys. B* **404**, 47–51 (2009). <https://doi.org/10.1016/j.physb.2008.10.016>
 22. R.K. Brow, R.J. Kirkpatrick, G.L. Turner, Nature of alumina in phosphate-glass 2. Structure of sodium aluminophosphate glass. *J. Am. Ceram. Soc.* **76**, 919–928 (1993). <https://doi.org/10.1111/j.1151-2916.1993.tb05315.x>
 23. M. Karabulut, E. Metwalli, R.K. Brow, Structure and properties of lanthanum-aluminium-phosphate glasses. *J. Non-Cryst. Solids* **283**, 211–219 (2001). [https://doi.org/10.1016/S0022-3093\(01\)00420-3](https://doi.org/10.1016/S0022-3093(01)00420-3)
 24. S.H. Morgan, R.H. Magruder, E. Silberman, Raman-spectra of rare-earth phosphate-glasses. *J. Am. Ceram. Soc.* **70**, C378–C380 (1987). <https://doi.org/10.1111/j.1151-2916.1987.tb04925.x>
 25. J.L. Rygel, Y.S. Chen, C.G. Pantano et al., Local structure of cerium in aluminophosphate and silicophosphate glasses. *J. Am. Ceram. Soc.* **29**, 4577–4582 (1994). <https://doi.org/10.1111/j.1151-2916.2011.04596.x>
 26. S.W. Lee, K.S. Ryoo, J.E. Kim et al., Structure and radiative properties of aluminophosphate glasses. *J. Mater. Sci.* **94**, 2442–2451 (2011). <https://doi.org/10.1007/BF00376281>
 27. T. Izumitani, H. Toratani, H. Kuroda, Radiative and nonradiative properties of neodymium doped silicate and phosphate-glasses. *J. Non-Cryst. Solids* **47**, 87–100 (1982). [https://doi.org/10.1016/0022-3093\(82\)90348-9](https://doi.org/10.1016/0022-3093(82)90348-9)
 28. S. Ouchani, J.C. Dran, J. Chaumont, Exfoliation and diffusion following helium ion implantation in fluorapatite: implications for radiochronology and radioactive waste disposal. *Appl. Geochem.* **13**, 707–714 (1998). [https://doi.org/10.1016/S0883-2927\(97\)00078-4](https://doi.org/10.1016/S0883-2927(97)00078-4)
 29. R.A. Martin, P.S. Salmon, C.J. Benmore et al., Structure of lanthanum and cerium phosphate glasses by the method of isomorphic substitution in neutron diffraction. *Phys. Rev. B* (2003). <https://doi.org/10.1103/physrevb.68.054203>
 30. A.G. Shikerkar, J.A.E. Desa, P.S.R. Krishna et al., Diffraction studies of rare-earth phosphate glasses. *J. Non-Cryst. Solids* **270**, 234–246 (2000). [https://doi.org/10.1016/S0022-3093\(99\)00583-9](https://doi.org/10.1016/S0022-3093(99)00583-9)
 31. G. Walter, G. Goerigk, C. Russel, The structure of phosphate glass evidenced by small angle X-ray scattering. *J. Non-Cryst. Solids* **352**, 4051–4061 (2006). <https://doi.org/10.1016/j.jnoncrysol.2006.08.012>
 32. R.K. Brow, R.J. Kirkpatrick, G.L. Turner, Local-structure of Xal₂O₃. (1-X)Napo₃ glasses—an Nmr and Xps study. *J. Am. Ceram. Soc.* **73**, 2293–2300 (1990). <https://doi.org/10.1002/chin.199044012>
 33. A. Stamboulis, R.G. Hill, R.V. Law, Characterization of the structure of calcium aluminosilicate and calcium fluoro-aluminosilicate glasses by magic angle spinning nuclear magnetic resonance (MAS-NMR). *J. Non-Cryst. Solids* **333**, 101–107 (2004). <https://doi.org/10.1016/j.jnoncrysol.2003.09.049>
 34. D.S. Brauer, N. Karpukhina, R.V. Law et al., Structure of fluoride-containing bioactive glasses. *J. Mater. Chem.* **53**, 27–30 (2012). <https://doi.org/10.1039/b900956f>
 35. J.K. Christie, A. Pedone, M.C. Menziani et al., Fluorine environment in bioactive glasses: ab initio molecular dynamics simulations. *J. Phys. Chem. B* **115**, 2038–2045 (2011). <https://doi.org/10.1021/jp110788h>
 36. J.K. Christie, R.I. Ainsworth, N.H. de Leeuw, Ab initio molecular dynamics simulations of structural changes associated with the incorporation of fluorine in bioactive phosphate glasses. *Biomaterials* **35**, 6164–6171 (2014). <https://doi.org/10.1016/j.biomaterials.2014.04.032>
 37. J.C. Du, L. Kokou, J.L. Rygel et al., Structure of cerium phosphate glasses: molecular dynamics simulation. *J. Am. Ceram. Soc.* **94**, 2393–2401 (2011). <https://doi.org/10.1111/j.1151-2916.2011.04514.x>
 38. R.I. Ainsworth, D.D. Tommaso, J.K. Christie et al., Polarizable force field development and molecular dynamics study of phosphate-based glasses. *J. Chem. Phys.* **137**, 234502–234509 (2012). <https://doi.org/10.1063/1.4770295>
 39. P. Jund, R. Jullien, Computer investigation of the energy landscape of amorphous silica. *Phys. Rev. Lett.* **83**, 2210–2213 (1999). <https://doi.org/10.1103/PhysRevLett.83.2210>
 40. A. Tilocca, N.H.D. Leeuw, Structural and electronic properties of modified sodium and soda-lime silicate glasses by Car-Parrinello

- molecular dynamics. *J. Mater. Chem.* **16**, 1950–1955 (2006). <https://doi.org/10.1039/B517362K>
41. G. Fan, J. Diao, L. Jiang et al., Molecular dynamics analysis of the microstructure of the CaO-P₂O₅-SiO₂ slag system with varying P₂O₅/SiO₂ ratios. *Mater. Trans.* **56**, 655–660 (2015). <https://doi.org/10.2320/matertrans.M2014363>
 42. J.K. Christie, A. Tilocca, Short-range structure of yttrium aluminosilicate glass for cancer radiotherapy: car-parrinello molecular dynamics simulations. *Adv. Eng. Mater.* **12**, B326–B330 (2010). <https://doi.org/10.1002/adem.200980081>
 43. E. Tang, D.D. Tommaso, N.H.D. Leeuw, An Ab initio molecular dynamics study of bioactive phosphate glasses. *Adv. Eng. Mater.* (2010). <https://doi.org/10.1002/adem.201080011>
 44. K. Vollmayr, W. Kob, K. Binder, Cooling-rate effects in amorphous silica: a computer-simulation study. *Phys. Rev. B: Condens. Matter* **54**, 15808–15827 (1996). <https://doi.org/10.1103/PhysRevB.54.15808>
 45. H. Inoue, A. Makishima, Structure of fluorophosphate glasses. *Comput. Aided Innov. N. Mater.* **23**, 907–910 (1991). <https://doi.org/10.1016/B978-0-444-88864-8.50192-8>
 46. G. Lusvardi, G. Malavasi, L. Menabue et al., Synthesis, characterization, and molecular dynamics simulation of Na₂O-CaO-SiO₂-ZnO glasses. *J. Phys. Chem. B* **106**, 9753–9760 (2002). <https://doi.org/10.1021/jp020321s>
 47. H.Y. Hou, G. Xie, S.R. Chen et al., Structure of molecular dynamics simulated NaF-AlF₃ melt. *Chin. J. Nonferrous Metals.* (2000). <https://doi.org/10.19476/j.ysxb.1004.0609.2000.06.031>
 48. G.G. Boiko, N.S. Andreev, A.V. Parkachev, Structure of pyrophosphate 2ZnO·P₂O₅-2Na₂O·P₂O₅ glasses according to molecular dynamics simulation. *J. Non-Cryst. Solids* **238**, 175–185 (1998). [https://doi.org/10.1016/S0022-3093\(98\)00693-0](https://doi.org/10.1016/S0022-3093(98)00693-0)
 49. C.R.A. Catlow, W.C. Mackrodt, *Computer Simulation of Solids* (Springer, Berlin, 1983). [https://doi.org/10.1016/0022-3115\(83\)90130-7](https://doi.org/10.1016/0022-3115(83)90130-7)
 50. D. Bingham, A.N. Cormack, C.R.A. Catlow, Rigid-ion potentials for SrF₂, CaF₂ and GdF₃. *J. Phys.: Condens. Matter* **1**, 1205–1212 (1998). <https://doi.org/10.1088/0953-8984/1/7/004>
 51. S.C. Hendy, A. Edgar, Structure of fluorochlorozirconate glasses using molecular dynamics. *J. Non-Cryst. Solids* **352**, 415–422 (2006). <https://doi.org/10.1016/j.jnoncrysol.2006.01.008>
 52. T.S. Bush, J.D. Gale, C.R.A. Catlow et al., Self-consistent interatomic potentials for the simulation of binary and ternary oxides. *J. Mater. Chem.* **4**, 831–837 (1994). <https://doi.org/10.1039/JM9940400831>
 53. S. Girard, J.D. Gale, C. Mellot-Draznieks et al., Derivation of interatomic potentials for gallophosphates from the GaPO₄-quartz structure: transferability study to gallosilicates and zeotype gallophosphates. *Chem. Mater.* **13**, 1732–1738 (2001). <https://doi.org/10.1021/cm001233s>
 54. U. Hoppe, G. Walter, R. Kranold et al., Structural specifics of phosphate glasses probed by diffraction methods: a review. *J. Non-Cryst. Solids* **263–264**, 29–47 (2000). [https://doi.org/10.1016/S0022-3093\(99\)00621-3](https://doi.org/10.1016/S0022-3093(99)00621-3)
 55. Z. Wu, C. Romano, A. Marcelli et al., Evidence for Al/Si tetrahedral network in aluminosilicate glasses from Al K-edge x-ray-absorption spectroscopy. *Phys. Rev. B* **60**, 9216–9219 (1999). <https://doi.org/10.1103/PhysRevB.60.9216>
 56. R.A. Martin, P.S. Salmon, D.L. Carroll et al., Structure and thermal properties of yttrium aluminophosphate glasses. *J. Physics-Condens. Matter* **20**, 527–534 (2008). <https://doi.org/10.1088/0953-8984/20/11/115204>
 57. R.A. Martin, G. Mountjoy, R.J. Newport, A molecular dynamics model of the atomic structure of dysprosium aluminophosphate glass. *J. Physics-Condens. Matter* **21**, 075102 (2009). <https://doi.org/10.1088/0953-8984/21/7/075102>
 58. S. Wegner, L.V. Wüllen, G. Tricot, The structure of aluminophosphate glasses revisited: application of modern solid state NMR strategies to determine structural motifs on intermediate length scales. *J. Non-Cryst. Solids* **354**, 1703–1714 (2008). <https://doi.org/10.1016/j.jnoncrysol.2007.10.034>
 59. J.J. Videau, A.E. Hadrami, C. Labrugère et al., Structural influence of alumina in Zn-Cd-Pb phosphate glasses. *Phys. Chem. Glasses* **48**, 363–372 (2007)
 60. R.K. Brow, Nature Of Alumina In Phosphate-Glass. 1. Properties Of Sodium Aluminophosphate Glass. *J. Am. Ceram. Soc.* **76**, 913–918 (1993). <https://doi.org/10.1111/j.1151-2916.1993.tb05315.x>